H_3,[114] 99.2 in Me_3Si-CH_3,[8] and 96.6 in $MeS-CH_3$.[103] The value of 98 used for H_2P-CH_3 is an average of the latter two compounds.

NH. The BDE in ammonia is 105.8. The value in H_3C-NH_2[112] is 98.4. We have assumed a value of 98 for all other NH bonds.

OH. The BDE in water is 118.0. The BDE in H_3C-OH[112] is 104.1, and we have assumed a value of 104 for all other OH bonds.

SiH. The BDE in silane is 90.3 ± 1.2.[115] This BDE is 89.6 in CH_3-SiH_3[8] and 86.3 in $H_3Si-SiH_3$.[8] We have used a value of 90 for all other substituents, since their electronegativity is closer to methyl than silyl.

PH. The BDE in phosphine is 82 ± 2. This value is obtained from the experimental heat of formation of PH_2,[9] corrected to 0° with scaled theoretical frequencies.[100] This value differs from the value of 84 given by the original workers.[9] Since substituents usually lower the BDE, we adopt a value of 80 for all other PH bonds.

SH. The BDE in hydrogen sulfide is 90.0. The BDE in H_3C-SH[103] is 89.0 ± 1.0. This value is used for all other SH bonds.

(113) Colussi, A. J.; Benson, S. W. *Int. J. Chem. Kinet.* **1977**, *9*, 307-316.
(114) Golden, D. M.; Benson, S. W. *Chem. Rev.* **1969**, *69*, 125-134.
(115) Doncaster, A. M.; Walsh, R. *Int. J. Chem. Kinet.* **1981**, *13*, 503-514.

Dimanganese Complexes of a Septadentate Ligand. Functional Analogues of the Manganese Pseudocatalase

P. Mathur,[†,‡] M. Crowder,[§] and G. C. Dismukes*[†]

Contribution from the Department of Chemistry, Princeton University, Princeton, New Jersey 08544, and IBM Instruments, Orchard Park, Danbury, Connecticut 06810.
Received January 5, 1987

Abstract: Two new dimanganese(II) complexes have been prepared and characterized as the first functional analogues of the manganese pseudocatalase enzyme of *L. plantarum* (Beyer, W. F.; Fridovich, I. *Biochemistry* **1986**, *24*, 6420). These have the formulas $Mn_2(L)Cl_3$ (**1**) and $Mn_2(L)(OH)Br_2$ (**2**) in which Cl^- and OH^-, respectively, serve as one of two bridging ligands, the other coming from the alkoxide group of the binucleating ligand *N,N,N',N'*-tetrakis(2-methylenebenzimidazolyl)-1,3-diaminopropan-2-ol (HL). The solution structure of these complexes has been characterized by EPR spectroscopy at both 34 and 9 GHz. This reveals the presence of two equivalent high-spin Mn(II) ions electronically coupled by a weak electron spin exchange interaction. Analysis of the axial zero-field splitting ($D = -0.072$ cm^{-1}) of this spin $S = 5$ complex in terms of the magnetic dipole interaction between the two Mn ions yields a lower limit to their separation of 3.2 Å. Cyclic voltammetry reveals that three separable oxidation processes occur for **2** at $E_p = 0.60$ V (A), 0.80 V (B), and 1.03 V (C), while **1** exhibits only two oxidations: a reversible one-electron process at 0.57 V (A) analogous to **2** and a second oxidation at 1.18 V corresponding to B + C. The hydroxide bridge in **2** thus appears to stabilize the Mn(III) oxidation state relative to Mn(II) in comparison with the chloride bridge in **1**. The binuclear complexes **1** and **2** decompose H_2O_2 catalytically with an initial rate for **1** proportional to $[H_2O_2]^2[Mn_2(L)Cl_3]^1$, while mononuclear Mn(II) is ineffective. The mechanism proceeds through the initial formation of the μ-oxo-containing Mn^{III} intermediate, $[Mn_2^{III}(L)(O)]Cl_2$, which is reduced by a second H_2O_2 to release O_2. A similar mechanism could be operating in the manganese pseudocatalase enzyme of *L. plantarum*, which is known to contain two Mn(III) per subunit and thus may have a binuclear Mn site.

Multinuclear manganese sites that are involved in the catalysis of reactions vital to biological systems are being steadily recognized and studied. Besides the photosynthetic water-oxidizing complex, which is known to utilize 4 Mn ions for the oxidation of water to molecular oxygen,[1] evidence has accumulated that the Mn site of the pseudo-catalase from *Lactobacillus planatrum* is comprised of two Mn ions per protein subunit.[2] This enzyme catalyzes the disproportionation of H_2O_2. Manganese has also been used as an effective probe of the structure of divalent ion sites, owing to its readily detected hyperfine structure seen by EPR. Chien et al. have used this feature to identify a binuclear metal ion site in the enzyme enolase.[3]

Thus there is compelling interest in the characterization of multinuclear manganese complexes in various oxidation states in order to unravel the more complex behavior of the biological sites by serving as models of the structural, spectral, or functional properties. Because of the lack of high-resolution structural data on the Mn sites in these enzymes, most efforts have focused on the characterization of spectral analogues.[4,5]

In the present study we have utilized a septadentate macrocyclic ligand, based on the benzimidazole group, which is capable of binding two metal ions via an alkoxide bridge. Earlier work has established the suitability of this ligand for binuclear copper complexes as models for hemocyanin.[6] The ligand *N,N,N',N'*-tetrakis(α-methylenebenzimidazolato)-1,3-diaminopropane-2-ol is a good chemical analogue for the imidazole residue of histidine, which is found as a ligand to manganese in the protein superoxide dismutase[7] and is believed to be found in the manganese pseudocatalase from *L. plantarum* (Beyer and Fridovich, private

[†] Princeton University.
[‡] Present address: Indian Institute Technology, Kanpur, India.
[§] IBM Instruments.

(1) (a) *Manganese in Metabolism and Enzyme Function*; Schramm, V. L., Wedler, F. C., Eds.; Academic: New York, 1986. (b) Dismukes, G. C. *The Organization and Function of Manganese in the Water-Oxidizing Complex of Photosynthesis*; Academic: New York, 1986; Chapter 16, p 275.
(2) (a) Kono, Y.; Fridovich, I. *J. Biol. Chem.* **1983**, *258*, 6015. (b) Beyer, W. F., Jr.; Fridovich, I. *Biochemistry* **1985**, *24*, 6460.
(3) Chien, J. C. W.; Westhead, W. C. *Biochemistry* **1971**, *10*, 3198.
(4) (a) Cooper, S. R.; Dismukes, G. C.; Klein, M. P.; Calvin, M. *J. Am. Chem. Soc.* **1978**, *100*, 7248. (b) Sheats, J. E. Czernuszewicz, R. S.; Dismukes, G. C.; Rheingold, A.; Petrouleas, V.; Stubbe, J. Armstrong, W. H.; Beer, R.; Lippard, S. J. *J. Am. Chem. Soc.* **1987**, *109*, 1435.
(5) (a) Lynch, M. W.; Hendrickson, D. N.; Fitzgerald, B. J. Pierpont, G. C. *J. Am. Chem. Soc.* **1984**, *106*, 2041. (b) Okawa, H.; Honda, A.; Nakamura, M.; Kido, S. *J. Chem. Soc., Dalton Trans.* **1985**, 59. (c) Wieghart, K.; Bossek, U.; Ventur, D.; Weiss, J. *J. Chem. Soc., Chem. Commun.* **1985**, 347.
(6) McKee, V.; Zvagulis, M.; Dagdigian, J. V.; Patch, M. G.; Reed, C. A. *J. Am. Chem. Soc.* **1984**, *106*, 4765-4772.
(7) Fridovich, I. *Annu. Rev. Biochem.* **1975**, *44*, 147.

0002-7863/87/1509-5227$01.50/0

Table I. The Allowed First-Order Transitions ($M \leftarrow M - 1$) for $S = 5$ in Axial Ligand Fields and in Strong Magnetic Fields

transition[a]	frequency[b]	intensity: area	intensity: peak
$\|5,0\rangle \leftrightarrow \|5,1\rangle$	$G - {}^1/_2D + (\mathcal{D}^2/2G)({}^{57}/_4 \sin^4\theta - 111\cos^2\theta\sin^2\theta)$	30	1.0
$\|5,-1\rangle \leftrightarrow \|5,-2\rangle$	$G - {}^3/_2D + (\mathcal{D}^2/2G)({}^{45}/_4 \sin^4\theta - 63\cos^2\theta\sin^2\theta)$	28	0.31
$\|5,-2\rangle \leftrightarrow \|5,-3\rangle$	$G - {}^5/_2D + (\mathcal{D}^2/2G)({}^{21}/_4 \sin^4\theta + 33\cos^2\theta\sin^2\theta)$	24	0.16
$\|5,-3\rangle \leftrightarrow \|5,-4\rangle$	$G - {}^7/_2D + (\mathcal{D}^2/2G)(-{}^{15}/_4 \sin^4\theta + 177\cos^2\theta\sin^2\theta)$	18	0.086
$\|5,-4\rangle \leftrightarrow \|5,-5\rangle$	$G - {}^9/_2D + (\mathcal{D}^2/2G)(-{}^{63}/_4 \sin^4\theta + 369\cos^2\theta\sin^2\theta)$	10	0.037

[a] Label $|S,M\rangle$: to construct the frequencies for $|S,-M\rangle \leftrightarrow |S,-M-1\rangle$ simply change the sign in front of the first-order term in D. [b] $G = g\beta H$; $D = \mathcal{D}(3\cos^2\theta - 1)$; area $= S(S+1) - M(M-1)$; peak intensity $\approx$ (area)$\{3\mathcal{D}(M - {}^1/_2)\}^{-1}$(constant).

Table II. The Half-Field Transitions ($M + 1 \leftrightarrow M - 1$) to Second Order for $S = 5$ in Axial Ligand Fields and in the Strong Magnetic Field Limit[a,b]

transition	frequency	intensity (G/D^2): area	intensity (G/D^2): peak
$\|5,+1\rangle \leftrightarrow \|5,-1\rangle$	$2G + (\mathcal{D}^2/G)({}^{57}/_4 \sin^4\theta - 111\cos^2\theta\sin^2\theta)$	30	
$\|5,+2\rangle \leftrightarrow \|5,0\rangle$	$2G + 2D + (\mathcal{D}^2/G)({}^{51}/_4 \sin^4\theta - 87\cos^2\theta\sin^2\theta)$	29	1.0
$\|5,+3\rangle \leftrightarrow \|5,+1\rangle$	$2G + 4D + (\mathcal{D}^2/G)({}^{33}/_4 \sin^4\theta - 15\cos^2\theta\sin^2\theta)$	26	0.45
$\|5,+4\rangle \leftrightarrow \|5,+2\rangle$	$2G + 6D + (\mathcal{D}^2/G)({}^{3}/_4 \sin^4\theta + 105\cos^2\theta\sin^2\theta)$	21	0.24
$\|5,+5\rangle \leftrightarrow \|5,+3\rangle$	$2G + 8D + (\mathcal{D}^2/G)(-{}^{39}/_4 \sin^4\theta + 273\cos^2\theta\sin^2\theta)$	14	0.12

[a] Reference 9. [b] $|S,M\rangle$; $D = \mathcal{D}(3\cos^2\theta - 1)$; $G = g\beta H$; area $= S(S+1) - M^2$; peak intensity $\approx$ (area)$\{6M\}^{-1}$(constant); $\mathcal{D}^2/G = 186$ G.

communication). The present paper summarizes the synthesis and characterization of two Mn(II) complexes derived from this ligand. The solution structure of these has been determined by EPR spectroscopy, owing to the formation of poor quality crystals unsuitable for X-ray diffraction studies on the solid. We also report kinetic studies demonstrating that these serve as functional models of the manganese site involved in the catalytic disproportionation of H_2O_2 in the pseudocatalase from *L. plantarum*.

Experimental Section

All chemicals were A.R. grade and used without further purification except for acetonitrile, which was dried by distillation from P_2O_5 and stored under Argon.

N,N,N′,N′-Tetrakis(2-methylenebenzimidazolyl)-1,3-diaminopropan-2-ol(HL). The ligand was synthesized by condensing 1,2-diaminobenzene with 2-hydroxy 1,2-diaminopropanetetracetic acid, utilizing the procedure reported earlier by Reed et al.[6] It was characterized by ^{1}H NMR in $CDCl_3$: δ (relative intensity) M, 7.65 (32); M, 7.25 (30); S, 4.12 (27); S, 2.65 (13).

[Mn_2(L)Cl_3] (1). The ligand, HL (0.25 mmol), was suspended in CH_3CN in a three-neck flask. A second small flask was attached to one arm via a gas-tight seal and contained 0.5 mmol $Mn(ClO_4)_2{\cdot}6H_2O$ in CH_3CN. After the system was purged with argon, 0.4 mmol of aqueous tetrabutylammonium hydroxide (TBAH, Aldrich) was added to the ligand flask and the contents stirred for 30 min. Upon transfer of the $Mn(ClO_4)_2{\cdot}6H_2O$ into the ligand solution a white turbidity was produced which immediately disappeared. The colorless solution was stirred for another 30 min, transferred to an argon-purged airless fritted funnel, and filtered under argon into an airless filtration flask containing 0.5 mmol of tetraethylammonium dichloride (TEACl), dissolved in CH_3CN. Any precipitate at this point was rejected. Upon addition of another 0.25 mmol of TEACl, a flocculent white percipitate formed. This was washed with CH_3CN several times and dried in vacuo (yield 40%). The two-step addition of chloride eliminated a monomeric Mn(II) complex, and other impurities. The samples for analysis were recrystallized from CH_3OH:butanol (8:1). Anal. Calcd for $C_{35}H_{33}ON_{10}Mn_2Cl_3$: C, 50.8; H, 3.9; N, 16.9; Cl, 12.9; Mn, 13.6. Found: C, 50.73; H, 4.23; N, 16.83; Cl, 13.6; Mn, 14.1.

[Mn_2(L)(OH)Br_2] (2). The preparative procedure is almost identical with that described above, except that a methanolic solution of TBAH is used as base and a single addition of 0.5 mmol of tetraethylammonium bromide is used to precipitate the compound. Anal. calcd for $C_{35}H_{33}ON_{10}Mn_2Br_2(OH){\cdot}2H_2O$: C, 45.06; H, 4.06; N, 15.02; Br, 17.10; Mn, 11.9. Found: C, 44.93; H, 3.69; N, 15.63; Br, 16.78; Mn, 12.33.

C, H, N, Cl, and Br analyses were by Galbraith Laboratory. Crystals of the chloro and bromo complexes were grown either by slow crystallization from acetonitrile/butanol solution or by slow diffusion of the halide ion into a reaction solution of Mn(II), ligand, and base. In both cases the crystals were large enough for X-ray diffraction but were too disordered for high-resolution work.

Instrumentation. IR spectra were obtained on a PE-283 spectrophotometer and a Digilab FTIR. Q-band EPR spectra were obtained with an IBM model ER/200D spectrometer. Electronic absorption, X-band EPR, and cyclic voltammetry were performed as described previously.[8]

Results

EPR Spectroscopy. Because of the absence of diffraction quality crystals, a detailed study of the solution structure was undertaken by EPR spectroscopy at both X-band and Q-band frequencies.

Q-Band EPR. Figure 1A illustrates the 34-GHz spectrum of the bromo derivative taken at 140 K as a butanol solution. At low resolution the spectrum is comprised of two groups of transitions: a symmetric group of intense transitions centered at $g = 2$ and labeled "Ia–d" and a second group of transitions at the half-field value of $g = 4$, which are much weaker in intensity and are labeled "IIa–c". This complex provides a textbook example of the EPR spectrum of a spin $S = 5$ particle exhibiting weak zero-field splitting relative to the external magnetic field. This structure could be predicted utilizing standard formulas found in the literature[9] and is illustrated by the stick spectra shown in Figure 1 (A–C). Peaks in group I arise from the allowed $\Delta M_s = 1$ transitions for an $S = 5$ particle having axially symmetric zero-field splitting. The appropriate hamiltonian for this spin system is given in eq 1, where D specifies the magnitude of the

$$\mathcal{H} = \beta H(g_\perp S_x \sin\theta - g_\parallel S_z \cos\theta) + D[S_z^2 - {}^1/_3 S(S+1)] \quad (1)$$

zero-field splitting term and θ specifies the angle between the external magnetic field and the principal axis of the zero-field splitting tensor. No evidence for clearly resolved g anisotropy could be seen, so we assumed $g_\parallel = g_\perp$. The frequency and intensities for these allowed transitions are listed in Table I, and the stick spectrum which these predict for the single orientation of $\theta = \pi/2$ is shown in Figure 1A. Hamiltonian eq 1 predicts the presence of a half-field transition with intensity proportional to $D^2/g\beta H$. This corresponds to the weak group of transitions, labeled "II" in Figure 1A and expanded in Figure 1C. The observed structure is precisely that which is predicted on the basis of the observed zero-field splitting found for the intense transitions given in group I. The frequencies and intensities of these $\Delta M_s = 2$ transitions are listed in Table II, and the stick spectrum predicted from these is illustrated in Figure 1C. The mean value of the zero-field splitting interaction constant, $|D|$, for both sets of transitions is 772 ± 33 G (0.072 ± 0.003 cm^{-1}). The g value for the Mn(II) ions were assumed to be isotropic and equal to the free spin value, as is typically found.

Contributions to the zero-field splitting may arise from the electronic quadrupolar interaction, anisotropic superexchange, and the magnetic dipole–dipole interaction between the Mn(II) ions. The first of these can be quite small ($\sim 10^{-2}$ cm^{-1}) for Mn(II)

(8) Mathur, P.; Dismukes, G. C. *J. Am. Chem. Soc.* **1983**, *105*, 7093.
(9) Abragam, A.; Bleaney, B. *Electron Paramagnetic Resonance of Transition Ions*; Clarendon: Oxford University, 1970; p 139 and 158.

ions,[9,10] while the large spin $S = {}^5/_2$ often necessitates consideration of the dipolar contribution. Anisotropic superexchange scales as the product of the magnitude of the g anisotropy times the isotropic superexchange and so should be insignificant in the present case. By attributing the major source of the observed zero-field splitting to the dipole–dipole interaction, a lower limit to the distance of separation between the Mn ions was obtained. The diagonal term for the zero-field splitting interaction has the angular dependence given by eq 2.

$$D = \mathcal{D}[(3g_{\parallel}^2/g^2)\cos^2\theta - 1] \quad (2)$$

The amplitude of this interaction is given by eq 3 with use of the point dipole approximation.[11] This yields a separation of R

$$\mathcal{D} = 6g^2\beta^2/4R^3 \quad (3)$$

$= 3.28 \pm 0.05$ Å. This separation can be compared to the Cu–Cu separation seen by X-ray diffraction in the analogous $[Cu_2(L\text{-}Et)X]^{2+}$ cations: 3.615 Å, $X^- = N_3^-$; 3.459 Å, $X^- = OAc^-$ (ref 6), and 3.325 Å, $X^- = NO_2^-$ (ref 14). Both acetate and azide bridge via 1,3-coordination while nitrite exhibits 1,2-coordination in these complexes. The integrated oscillator strength of the allowed transitions is predicted by eq 4 and should correspond to the areas under each peak between $\theta = 0$ and $\pi/2$. These are

$$|\langle S,M|S^+|S,M-1\rangle|^2 = S(S+1) - M(M-1) \quad (4)$$

listed in Table I. Because of the angular dependence of the zero-field splitting, these absorption intensities will not necessarily correspond to the observed derivative peak heights in the experimental spectra. To account for this in the simulation the angular dependence of the probability of absorption was considered explicitly. The probability that an EPR transition will occur in the interval between H and dH is proportional to $\sin\theta\, d\theta$, as given in eq 5. Using this expression and the expression for $dH/d\theta$

$$P(H)\, dH \propto \sin\theta\, d\theta \quad (5)$$

obtained from the resonance frequency equations in Tables I and II, one obtains eq 6 for the angular dependence of the transition probability.

$$P(H) \propto \frac{g\beta}{\mathcal{D}\cos\theta} \quad (6)$$

This gives the usual angular dependence for an axial tensor showing that it is most probable to find the magnetic field oriented perpendicular rather than parallel to the unique molecular axis. It is this intensity function that is plotted as a function of θ for the predicted transitions in Figure 1. A comparison with the experimental spectra indicates that the qualitative distribution of intensities is satisfactory; the major difference being the presence of greater intensity in the central peaks of the experimental spectrum (Figure 1A). This is possibly due to the population of the spin $S = 4$, 3, 2, and 1 states which should contribute spectra analogous to the $S = 5$ state, except with 1, 2, 3, and 4 fewer pairs of outer transitions, respectively, governed by the absence of the higher M_s sublevels in these states (Table I).

Hyperfine structure is resolved on the central transition labeled Ia and Ia′, as shown in Figure 1B. This structure consists of a symmetric group of 11 lines superimposed on each of the peaks labeled Ia and Ia . Each is characterized by a nearly constant hyperfine splitting of 45 ± 3 G and a distribution of peak intensities that approximates the nearly integral distribution of peak intensities expected for two-coupled spin $I = {}^5/_2$ nuclei, as is the case for ^{55}Mn (1:2:3:4:5:6:5:4:3:2:1). The hyperfine coupling constant of 45 G is half that of a typical Mn(II) coupling constant found in monomeric complexes and is diagnostic for a pair of exchanged coupled Mn(II) ions.[8] A stick spectrum of the predicted hyperfine structure as shown in Figure 1B agrees well with the observed peak positions and intensities.

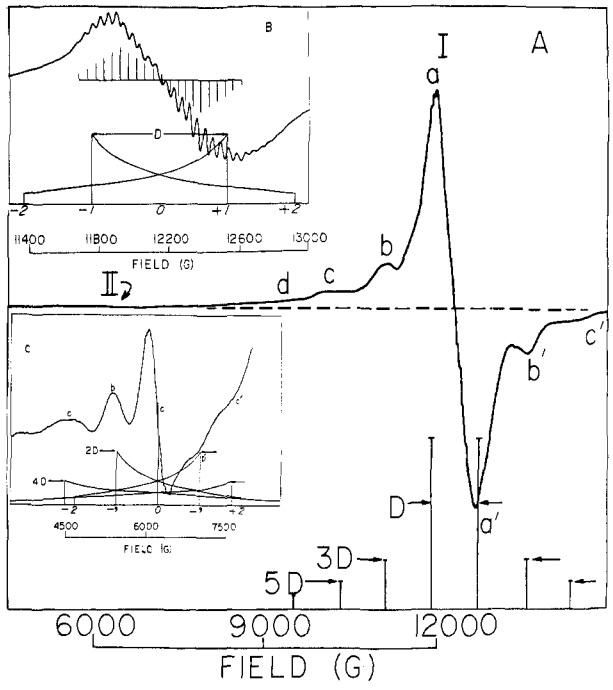

Figure 1. (A) Q-band EPR spectrum of the complex **2** in *n*-butanol at 140 K; microwave frequency, 34 GHz; microwave power, 22.0 mW. The stick spectrum of region I a–d for the case $\theta = \pi/2$ is shown below. (B) A 2000-G scan of the spectrum in part A centered at 12 200 G. The lower traces give the predicted angular dependence of the two transitions Ia and Ia′, while the stick spectrum above this gives the hyperfine structure for two ^{55}Mn nuclei. (C) A 5000-G scan of the spectrum in part A centered at 6000 G to illustrate the weak half-field transitions in group II. The lower trace gives the predicted angular dependence for $0 \le \theta \le \pi/2$ of the five half-field transitions from Table II.

Mononuclear Mn(II) impurities arise when fewer than four benzimidazole groups form per ligand. The resulting Mn(II) species can be identified by EPR from its zero-field splitting (apparent g values (5, 1.7, 1.2) which are typical of Mn(II) ions in trigonal symmetry (UnniNair & Dismukes, unpublished)). These are eliminated by using the purification scheme given in the Experimental Section.

In conclusion, we find that EPR spectroscopy provides clear evidence for the presence of a pair of magnetically equivalent high-spin Mn(II) ions separated by 3.3 Å and coupled via an electronic exchange interaction fostered by shared bridging ligands. These data provide a partial view of the manganese site in solution and suggest the cationic structure I. This differs from the $[Cu_2(L\text{-}Et)X]^{2+}$ cations[6,14] by placing all three chlorides as inner-sphere ligands coordinated to manganese. Both IR and electrochemical evidence support this structure.

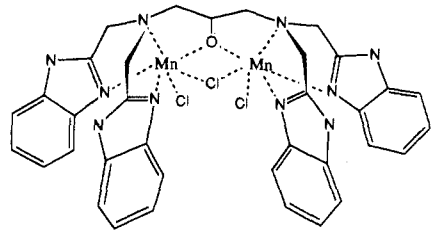

X-Band Spectra. A temperature-dependence study was conducted at X-band in order to determine the energy level structure. The 10-GHz EPR spectra of the chloro and bromo derivatives as butanol solutions at 100 K are nearly identical, as shown in Figures 2B and 3B, respectively. This means that the dipolar interaction between the manganese ions is the same in the two

(10) Carlin, R. L.; van Duyneveldt, A. J. *Magnetic Properties of Transition Ions*; Springer-Verlag: New York, 1977; p 201.
(11) Carrington, A.; McLachlan, K. *Introduction to Magnetic Resonance*; Methuen: New York, 1979; p 130.
(12) Steck, E. A.; Nachod, F. C.; Ewing, G. W.; Gorman, N. H. *J. Am. Chem. Soc.* **1948**, *70*, 3406.
(13) Lane, T. J; Nakagawa, I.; Walter, J. L.; Kandathil, A. J. *Inorg. Chem.* **1962**, *1*, 267.
(14) McKee, V.; Zvagulis, M.; Reed, C. A. *Inorg. Chem.* **1985**, *24*, 2914.

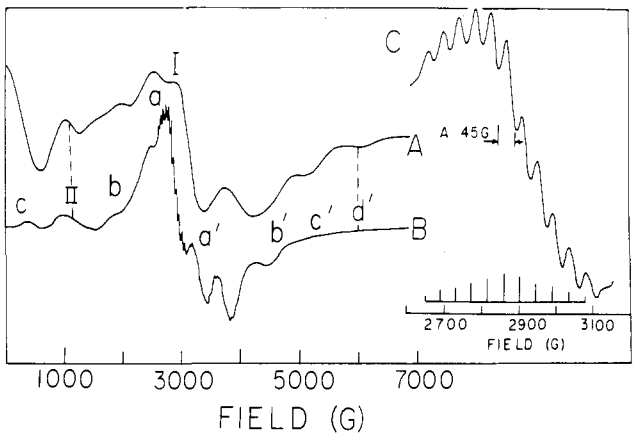

Figure 2. (A) A 10000-G scan of complex **1** in *n*-butanol at $T = 9.5$ K. Microwave power, 0.5 mW; microwave frequency, 9.28 GHz; modulation amplitude of 5.0 G; gain 2000. (B) $T = 120$ K; microwave power, 10.0 mW; microwave frequency, 9.05 GHz; gain 200. (C) A 1000-G scan of the spectrum in part B, centered at 2800 G, showing the hyperfine structure from two ^{55}Mn nuclei.

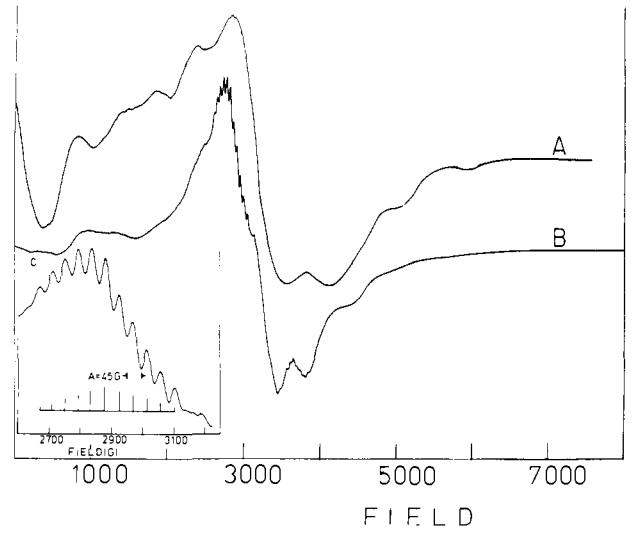

Figure 3. (A) A 10000-G scan of complex **2** in *n*-butanol at $T = 9.5$ K. Microwave power 0.5 mW; microwave frequency, 9.21 GHz; 5.0 G modulation amplitude; gain 2500. (B) $T = 120$ K; microwave power 10.0 mW; microwave frequency 9.05 GHz; 8.0 G modulation amplitude; gain 250. (C) A 1000-G scan of the spectrum in part B centered at 2750 G, showing hyperfine structure.

complexes so that the Mn(II) ions are separated by the same distance. The essentially identical zero-field splitting of **1** and **2** is consistent with the view that OH^-, rather than Br^-, serves as the bridging ligand between the Mn(II) ions in **2**.

A quantitative simulation of these spectra is not possible utilizing the equations given in Tables I and II, owing to the fact that the strong field approximation is no longer valid at the X-band frequency. On the other hand, the comparatively narrow ^{55}Mn hyperfine structure, as seen in Figures 2C and 3C, conforms to the first-order behavior and is readily predicted by the previous binuclear model, shown by the stick spectra. The average hyperfine splitting constant for both complexes is 43 ± 3 G, in close agreement with the Q-band data. In contrast with the Q-band data, the hyperfine structure is well resolved on only one zero-field peak, suggesting evidence for unresolved anisotropic interactions.

By studying the temperature dependence of the EPR signal intensity it is possible to determine the sign and possibly estimate the size of the electronic coupling between the manganese ions. Figures 2A and 3A illustrate the relative changes in the spectra observed upon lowering the temperature to 10 K. The spectra were recorded under conditions where microwave power saturation did not occur so that the intensities are representative of the state populations.

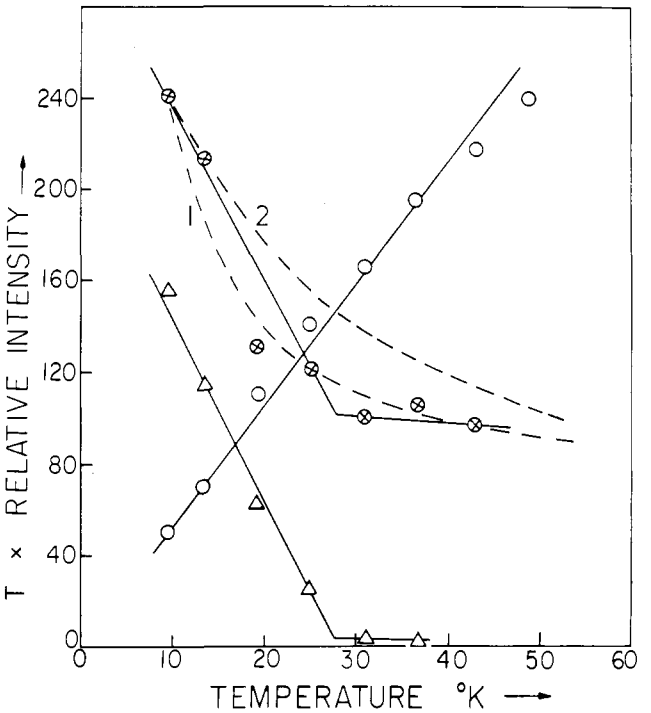

Figure 4. Plot of the relative intensity × T, calculated as the product peak amp × (line width) × T plotted vs. temperature, for complex **1**. Open circle (○) represents the central peak at 3200 G; triangle (△) represents the low field peak at 0–600 G; while the circles with crosses (⊗) represent the high field peak at 5100 G. The dashed curves are calculated from eq 7 with use of $D = -0.072$ cm^{-1} and $J = -0.7$ cm^{-1} (curve 1) and $J = -2.8$ cm^{-1} (curve 2).

The qualitative result which is seen from these figures is that the intensity centered at $g = 2$ near 3200 G is reduced, relative to the intensity in the wings of the spectra at both lower and higher fields. This is in accord with predictions on the energy level structure used to quantitatively interpret the Q-band structure. The sign of D determines the relative order in energy of the $2S + 1$ magnetic sublevels (M) for each level characterized by spin S. For the $S = 5$ level at zero-field, a negative value of D places the $M = 0$ level highest in energy and the $M = \pm 5$ levels lowest in energy. At low temperatures when kT is comparable with the overall splitting the population of the highest levels will be noticably reduced. The intensity of the transitions in these levels will decrease relative to those between the lower levels.

To examine this the temperature dependence of several of the peaks of the EPR spectrum was followed between 10 and 50 K. The results shown in Figure 4 are plotted as intensity × temperature. They indicate that the central transitions, corresponding to low M_s sublevels, exhibit a monotonic inverse temperature dependence compared with the high-field and low-field peaks (larger $|M|$). An attempt to predict the temperature dependence of these EPR transitions was performed. The temperature dependence for the population of the 38 states arising from the pair of coupled $S_i = {}^5/_2$ Mn(II) ions was calculated as $P_i(S,M)$ and multiplied by the oscillator strength expression (OSC) to arrive at the EPR intensity in eq 7.

$$\mathrm{Int}_i = \mathrm{OSC}_i \times P_i(S,M)$$

$$P_i(S,M) = \frac{e^{-[E_i(S,M)-E_0]/kT} - e^{-[E_i(S,M-1)-E_0]/kT}}{\mathrm{ZTOT}} \qquad (7)$$

$$\mathrm{OSC}_i = S(S+1) - M(M-1)$$

$$\mathrm{ZTOT} = \sum_i^{38} e^{-[E_i(S,M)-E_0]/kT}$$

The energy expression used in $P_i(S,M)$ was taken from eq 1 (Table I) and included the exchange energy term $2J\mathbf{S}_1\cdot\mathbf{S}_2$ ($E_J = JS(S + 1) - {}^{35}/_2$) to account for the separation of states of different total spin. By fixing D at the value deterined from Figure 1, an

Table III. Observed IR Frequencies (cm^{-1}) and Proposed Modes of Assignments for the Ligand and the Complexes[a]

HL	$[Mn_2^{II}(L)Cl_3]$	$[Mn_2^{II}(L)(OH)Br_2]$	assignment
1620 s	1620 s	1615 s	ν(C=N)
1525 s	1525 s	1530 s	L
1430 vs, br	1445 vs, br	1450 vs, br	ν_s(C=N=C=C—)
1445 sh	1465 sh	1468 sh	L
1480 w	1485 sh	1488 sh	L
1350 s	1382 s	1385 s	δ(—O—H)
1305 s	1328 s	1330 s	δ(R_3C—H)
1270 s	1272 s	1275 s	L
1215 s			L
1120 m	1110 w	1120–1115	L
1060 m			ν(C—O)
1020 m	1032	1035	ν(C—O)
740 vs, br	740 vs, br	745 vs, br	L
650 w	650 w	660 w	L
610 m			L
		580 m	ν(Mn—OH)
470 m	470 m	470 m	L
430 m	430 m	430 m	L
285 sh			L
	265 w		ν(Mn—Cl)
252 w			L

[a] Symbols: ν_s = stretch, δ = deformation, br = broad, L = ligand, m = medium, s = strong, sh = shoulder, vs = very strong, w = weak.

estimate of J could be made. The dashed curves labeled 1 and 2 in Figure 4 refer to the predicted behavior for the $|5,5\rangle \rightarrow |5,4\rangle$ transition for the cases $J = -0.7$ and -2.8 cm^{-1}, respectively. The case for $J > 0$ gives only an increase of intensity $\times$ T with T. These data suggest a weak ferromagnetic coupling between the two Mn(II) ions with $|J| \sim 1$ cm^{-1}. This method can give only an approximate magnitude for J, since it relies on an energy expression that is appropriate for a fixed magnetic field. The field is actually different for each transition. The central transitions near $g = 2$ probably represent the overlap of a number of transitions from different spin states. No attempt was made to simulate these.

Electronic Spectroscopy. The ligand in butanol has three prominent absorption bands, λ_{max} 251, 275, and 282 nm, with extinctions of log ϵ = 4.44, 4.58, and 4.61, respectively. No absorption band was observed for the ligand above 300 mm, as is also true for free benzimidazole and 2-dialkyl amino methyl derivatives.[12]

Both manganese complexes exhibit absorption maxima at 242, 273, and 280 nm with extinctions of log ϵ = 4.26, 4.47, and 4.51 ($Mn_2^{II}(L)Cl_3$) and 4.27, 4.37, and 4.42 ($Mn_2^{II}(L)(OH)Br_2$). The bromo complex has a weak shoulder at 335 nm, while no such feature is present for the chloro complex. Neither complex absorbs in the visible, as is typical for Mn(II) complexes.

Infrared Spectroscopy. Selected IR transitions for the ligand and the manganese complexes are summarized in Table III. In the free ligand, a strong band is found at 1430 cm^{-1} with two other weaker bands at 1445 and 1480 cm^{-1}. On the basis of the analogy with the assigned bands for imidazole, the 1430-cm^{-1} band is attributable to the symmetric stretching mode for (-C=N—C=C-), while the other two are overtone or combination bands.[13] In the complexes, the 1430-cm^{-1} band shifts to 1445 cm^{-1} (chloro) and 1450 cm^{-1} (bromo), implying direct coordination of all four imine nitrogens to manganese. This is the preferred nitrogen atom for coordination in other metal complexes with benzimidazole.[14]

The in-plane deformation mode for an OH group belonging to a secondary alcohol is characterized in the region 1350–1260 cm^{-1},[15] and that for a tertiary CH is characterized at 1340 cm^{-1}.[16] In the free ligand two strong bands at 1350 and 1305 cm^{-1} are attributable to these vibrational modes. Stirring the ligand with D_2O severely diminishes the 1350-cm^{-1} band, identifying it with a labile proton attributed to be the OH group. In the complexes, the 1350-cm^{-1} band is absent, while in its place a new band appears at 1382 cm^{-1} (chloro) and 1385 cm^{-1} (bromo), suggesting deprotonation of OH and coordination to Mn(II). The 1305-cm^{-1} band shifts to 1328 cm^{-1} (chloro) and 1330 cm^{-1} (bromo) upon complex formation. Furthermore, if the bromo complex is prepared in the presence of D_2O, among other changes it shows a strongly diminished band at 1330 cm^{-1} (with concomitant enhancement of intensity of a band located at 978 cm^{-1}), attributable to the partial deuteriation of the proton at C(2). A shift of the same magnitude is observed for a manganese bound methoxyl group upon deuteriation.[17] A new band arises in the complexes at 1030 cm^{-1}, and this probably corresponds to the C–O stretch of the coordinated alkoxyl. The C–O stretch of metal bound methoxyl groups has been assigned at 1030–1050 cm^{-1}.[18]

A weak band at 265 cm^{-1} is observed for the chloro complex, which is absent in both the free ligand and the bromo complex. It can be assigned to a terminal Mn–Cl stretch, on the basis of values reported for other Mn^{II}–chloride complexes in the same region.[19]

Unfortunately, we were unable to directly assign a bridging chloride mode in the case of the chloro complex because of overlapping bands. Nonetheless, we tentatively assign a band at 580 cm^{-1} in the bromo complex to a bridging hydroxide. This band does not exist in either the free ligand or the chloro complex. Similar OH-bridged bimetallic complexes exhibit frequencies in the same region.[20,21] The IR data are consistent with the analytical data which establish the presence of two Br and one OH per ligand in the bromo complex. The absence of the 580-cm^{-1} IR band and the stoichiometry of 3 Cl per ligand in the chloro complex indicate that Cl is the likely bridging atom in this derivative.

Electrochemistry. Cyclic voltammograms were recorded in a mixed-solvent system (CH_3CN:butanol) owing to the insolubility of the compounds in CH_3CN, and unlike the high solubility of the cationic $[Cu_2(L)X]^{2+}$ complexes in CH_3CN.[6] This result supports the IR data, showing that the chlorides are inner-sphere ligands even in solution. The stability of the binuclear structure in this mixed solvent was confirmed by the identical EPR features as found in pure butanol (EPR section). Also, both Cl^- and Br^- ions remained coordinated to manganese in the mixed-solvent system, since no waves coincident with solvated Cl^- or Br^- ions were detected. The complexes are increasingly unstable in the following series of primary alcohols: $(CH_3)_2CHOH$, CH_3CH_2OH, and CH_3OH. The electroactivity of butanol on a Pt electrode was also checked; an oxidation process above +1.40 V and a reduction below −0.40 V vs. SCE were observed. The redox processes for the complexes are in a region (0.0 to +1.20 V) free from solvent interference. Ferrocene was used as internal standard, yielding the Fc/Fc^+, one-electron couple at E_m = +0.40 V vs. SCE, with a peak-to-peak separation of 130 mV.

The cyclic voltamograms of **1** and **2** are shown in Figure 5. The voltammogram of **2** shows three oxidation processes at E_p = 0.60, 0.80, and 1.03 V, while **1** shows two resolved oxidation processes occurring at E_p = 0.57 and 1.18 V. The first wave in both complexes is nearly reversible, with E_m = 0.54 V and width = 110 mV for **2** while E_m = 0.49 V and width = 150 mV for **1**. This process is consistent with a one-electron oxidation to form the mixed-valence Mn_2(II,III) species.

Of the other two oxidation processes in the case of **2** the wave at 0.80 V is irreversible, while the wave at 1.03 V is associated with a reduction wave at 0.85 V. They are also tentatively assigned as one-electron oxidation processes forming the Mn_2(III,III) and the Mn_2(III,IV) states, although we have no direct evidence to support this. For **1** the oxidation wave at 1.18 V is associated

(15) Tanaka, C.; Kuratani, K.; Mizushima, S. *Spectrochim. Acta* **1957**, *9*, 265.
(16) Vogel, A. I. *Textbook of Practical Organic Chemistry*; Longman: London, 1978; p 1271.
(17) Camenzind, J. M.; Hollander, F. F.; Hill, C. L. *Inorg. Chem.* **1982**, *21*, 4301–4308.
(18) Maslowsky, E. *Vibrational Spectra of Organometallic Compounds*; Wiley: New York, 1977.
(19) Frank, W. C.; Rogers, L. B. *Inorg. Chem.* **1966**, *5*, 615.
(20) Maroni, V. A.; Spiro, T. G. *Inorg. Chem.* **1968**, *7*, 183.
(21) Maroni, V. A.; Spiro, T. G. *J. Am. Chem. Soc.* **1966**, *88*, 1410.

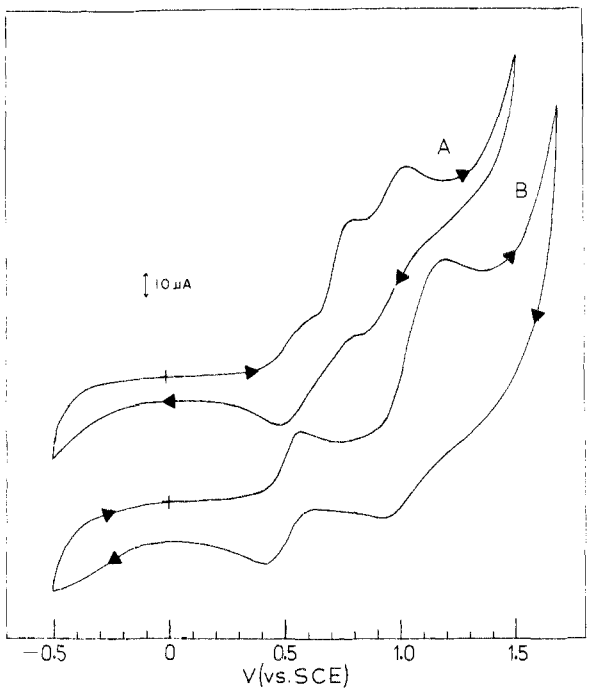

Figure 5. (A) Cyclic voltammogram of complex **2** (10^{-3} M) in 1:4.5 butanol/acetonitrile. Tetrabutylammonium perchlorate (0.1 M) supporting electrolyte; scan rate 100 mV/s vs. SCE. (B) Cyclic voltammogram of complex **1** with the same conditions as given in part A. Scan rate 50 mV/s.

with a reduction at 0.93 V. The peak current is approximately the sum of the currents found for the peaks at 0.80 and 1.03 V in **2**. The peak-to-peak separation is 0.25 V, which is well above the width for a one-electron couple. Therefore, it appears to be a merging of the two resolved oxidation processes seen in the **2**, corresponding to the formation of Mn_2(III,IV) from Mn_2(II,III). This wave is shifted positively by +150 mV with respect to the Mn_2(III,III)/Mn_2(III,IV) couple and by 380 mV relative to the Mn_2(II,III)/Mn_2(III,III) couple for **2**. It thus appears that chloride in **1** destabilizes the higher oxidation states of manganese relative to the μ-hydroxide structure of **2**.

Reactivity with H_2O_2. Hydrogen peroxide decomposes catalytically in the presence of either complex; a kinetic investigation of the mechanism was carried out with the chloro complex. The insolubility, or instability, of the complex in common water miscible organic solvents precludes examination of the kinetics in a homogeneous phase, and consequently the reaction was carried out in a two-phase system.

The complex was dissolved in butanol and allowed to react at a constant stirring rate and surface area with an aqueous layer of H_2O_2 in a vessel fitted with a stopcock. By monitoring the gas evolved volumetrically at 1-min intervals, a typical kinetic curve was obtained; an initial rate was determined at 3.0 min, using the method of tangents. The H_2O_2 phase was unbuffered, and the initial pH was 4.3 and rose to 6.1 upon completion of the reaction ($t > 15$ min). Attempts to use acetate and phosphate buffers caused extraction of Mn(II).

The dependence of the initial rate of gas evolution on the initial concentration of the complex is linear as shown in Figure 6A. On the other hand, the initial rate depends linearly on the square of the initial H_2O_2 concentration, as shown in Figure 6B. The reaction rate slows as the reaction proceeds, attributable at least partially to destruction of the complex. This was verified by an examination of the aqueous phase by EPR, which showed the presence of hexaquo Mn(II). Over this time the complex reacts with protons as judged from the increase in the initial unbuffered pH from 4.3 to 6.1 at the end of reaction. Typically 200 mmol of H_2O_2 are decomposed per 1 mmol of [Mn_2(L)Cl_3].

As the H_2O_2 decomposition proceeds the butanol layer turns yellow. The optical spectrum of the yellow intermediate closely

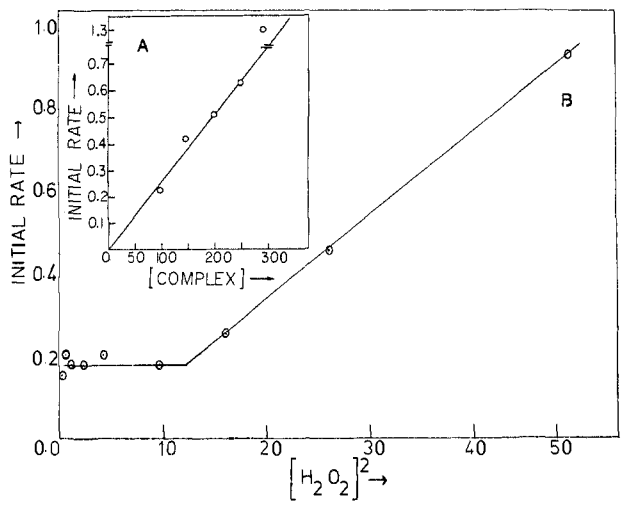

Figure 6. (A) Plot of initial rate of O_2 evolution vs. the initial concentration of complex **1**. (B) The initial rate of O_2 evolution vs. the square of the initial concentration of H_2O_2.

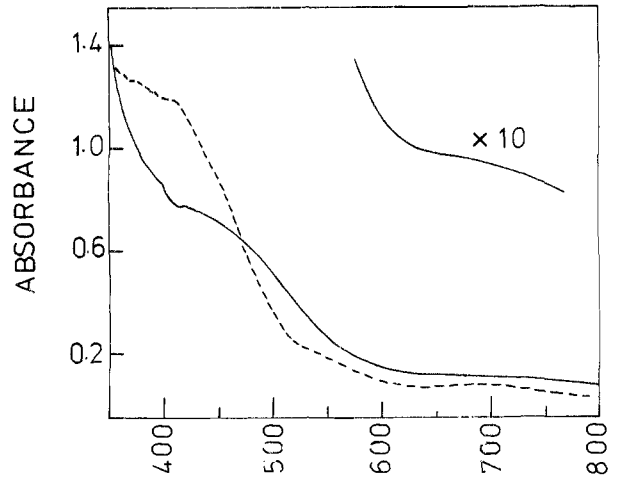

Figure 7. The visible electronic spectrum of the peroxide oxidation intermediate of Mn_2(L)Cl_3 (solid trace) and of the μ-oxo periodate oxidation product (dashed curve). The absorbance scale is arbitrary.

resembles that of the $Mn_2^{III,III}$(L)(μ-O) species (Figure 7) obtained upon oxidation of 2 mmol of Mn(II) by 1 mmol of periodate in the presence of 1 mM of HL and precipitation of the product with excess perchlorate. The assignment of this product as an oxo-bridged species is based upon the IR spectrum, which exhibits three very strong bands at 698, 655, and 620 cm^{-1}. Three of the vibrational modes of the 4-membered ring, Mn_2O_2, have been assigned in the 600–700-cm^{-1} region in related Mn(III) and Mn(IV) complexes.[4b,22]

A frozen solution of the yellow intermediate is EPR silent at 10 K and above, implying the formation of an even-spin species such as Mn(III). Furthermore, when this is reacted with a two-electron reducing agent like cathechol, and a frozen solution is examined by EPR, features of the parent Mn_2(II,II) complex reappear. This implies that the yellow intermediate is a two-electron oxidized product, consistent with the formation of the Mn_2(III,III) oxidation state. This oxidation is thermodynamically viable if we compare the redox potential of the couple H_2O_2/H_2O, which is 1.30 V vs. SCE at pH 4.0,[23] with that of the second oxidation wave in the voltammogram of the chloro complex, E_{peak} = 1.18 V vs. SCE in CH_3CN/butanol.

The optical, IR, and EPR data taken together imply the formation of a $Mn_2^{III,III}$(L)(μ-O) complex upon oxidation by H_2O_2, eq 8; further reaction of this intermediate with another H_2O_2

(22) Cooper, S. R.; Calvin, M. *J. Am. Chem. Soc.* **1977**, *99*, 6623.
(23) Bray, W. C. *Chem. Rev.* **1932**, *10*, 161.

molecule in the rate-determining step (eq 9) of O_2 release provides a rational explanation of the kinetic results. An increase in pH

$$[Mn_2^{II}(L)Cl_3] + H_2O_2 \rightleftarrows [Mn_2^{III}(L)(O)Cl_3] + H_2O \quad (8)$$

$$[Mn_2^{III}(L)(O)Cl_3] + H_2O_2 \rightarrow [Mn_2^{II}(L)Cl_3] + H_2O + O_2 \quad (9)$$

over the course of the reaction accompanies the loss in O_2 evolution. This could be due to the protonation of the ligand which decomposes the binuclear structure and produces free Mn(II) in the aqueous phase.

The catalytic nature of the above reaction is attributable to the stability of the binuclear manganese site, which is derived from the binucleating ligand structure. In contrast, the series of binuclear Mn(III) and Mn(IV) complexes ($Mn_2^{III}(O)(CH_3CO_2)_2(Pz_3BH)_2$ and $Mn_2^{IV}O_2(bipy)_4$) decomposes H_2O_2 in homogeneous solutions by reactions that are stoichiometric at best (Mori, Sheats, and Dismukes, unpublished). This can be explained by the instability of the reduced states toward dissociation of the Mn ions in the absence of a binucleating ligand. Also, mononuclear Mn(II) in solution did not decompose H_2O_2 over the same interval, again indicating the need for the redox capacity found in two Mn ions.

The manganese-containing pseudocatalase of *L. plantarum* decomposes H_2O_2 by a mechanism that was originally believed to involve the cycling between Mn(III) and Mn(V) oxidation states on a single ion.[2a] Since this earlier report it has been learned that the enzyme contains 2 Mn(III) ions per protein subunit[2b] and that the site is probably binuclear (Fridovich and Beyer, private communication). We suggest that the mechanism of this biological reaction may also involve chemistry which parallels that given in reactions 8 and 9.

Acknowledgment. This work was supported by a grant from the National Science Foundation (CHE82-17920). We thank Dr. B. C. UnniNair, who was involved in preliminary studies on this project. G.C.D. acknowledges support from the A. P. Sloane Foundation.

Dihydridotetrakis(pyrophosphito(2-))diplatinate(III)

Erica L. Harvey, Albert E. Stiegman, Antonín Vlček, Jr.,[1] and Harry B. Gray*

Contribution No. 7557 from the Arthur Amos Noyes Laboratory, California Institute of Technology, Pasadena, California 91125. *Received February 13, 1987*

Abstract: The $d\sigma^*p\sigma$ triplet excited state of $[Pt_2(P_2O_5H_2)_4]^{4-}$ (Pt_2) reacts with hydrogen-atom donors to give Pt_2H_2. NMR (^1H and ^{31}P) and IR spectroscopic studies show that Pt_2H_2 is an axial dihydride: $^2J_{P-H}$, 11 Hz; $^3J_{P-H}$, 3.7 Hz; $^1J_{Pt-H}$, 884 Hz; $^2J_{Pt-H}$, 103 Hz; $^3J_{H-H}$, 26 Hz; $^2J_{P-O-P}$, >42 Hz; $^1J_{Pt-P}$, 2190 Hz; $^1J_{Pt-Pt}$, ~8000 Hz; ν(Pt-H), 1840 cm^{-1}. Reactions of Pt_2H_2 include photochemical release of H_2, rapid thermal reduction of O_2, and thermal reduction of HCl to H_2.

Hydrogen-atom transfer has been established as an important reaction pathway for the $d\sigma^*p\sigma$ triplet excited state of $[Pt_2(P_2O_5H_2)_4]^{4-}$ (Pt_2).[2-4] Substrates that serve as H-atom donors include alcohols with α(C-H) bonds[2,3] and triorganosilanes, -germanes, and -stannanes.[4] These substrates all react photochemically with Pt_2 upon 370-nm irradiation to produce the same complex,[3] which is characterized by strong absorption at 314 nm. NMR and IR spectroscopic studies reported here show that the common photoproduct is a binuclear platinum(III) dihydride, $[Pt_2(P_2O_5H_2)_4H_2]^{4-}$ (Pt_2H_2).

Experimental Section

The title compound (Pt_2H_2) is generated by 370-nm narrow-band irradiation of freeze-pump-thaw degassed acetonitrile solutions of $[Bu_4N]_4[Pt_2(P_2O_5H_2)_4]$ containing the hydrogen-atom donor.[4] The extent of the photoreaction and stability of the photoproduct strongly depend on the nature of the substrate; Pt_2H_2 usually decomposes thermally, regenerating Pt_2 by reaction with unreacted substrate as well as with other photoproducts. We have found that Pt_2H_2 is reasonably stable only when generated by photolysis of either Bu_3SnH, $PhCH(OH)CH_2CH_3$, or $PhCH(OH)CH_3$ with Pt_2. The latter H donor was used in all experiments described here because conversion of Pt_2 to Pt_2H_2 at concentrations as high as 0.04 M was achieved (the half-life of Pt_2H_2 is at least 1.5 weeks in this case). The alcohols were purchased from Aldrich and distilled before use. Acetonitrile (B and J High Purity Solvent) and CD_3CN (Aldrich Gold Label) were used as received. Both ^1H and ^{31}P NMR spectra were obtained on a 400-MHz JNM-GX400 FT NMR spectrometer after direct irradiation of a vacuum-sealed 10-mm NMR tube containing Pt_2 and $PhCH(OH)CH_3$. The IR spectrum was taken on a Beckman IR 4240; for this experiment the photoproduct was generated in a photolysis cell and transferred to the IR cell in a rigorous N_2 atmosphere. A Shimadzu UV-260 spectrometer was used to record the UV-vis absorption spectra. The composition of the atmosphere above the irradiated solutions before and after reaction with HCl and DCl was analyzed by mass spectrometry; the stoichiometry of release of H_2 during photolysis of the intermediate was measured by Toepler pumping.

Computer simulations were performed by using the Nicolet NMRSIM program at the Southern California Regional NMR Facility at Caltech. Due to the prohibitive number of spins (10-12) in the actual isotopomers, smaller spin systems (≤ 7) were studied extensively and the results were extrapolated where possible. For example, $J_{P-O-P} > 42$ Hz produces a triplet in the ^1H spectrum of an AA'XX' (A = ^1H; X = ^{31}P) spin system and a quintet with the same splitting in the ^1H spectrum of an AA'XX'X''X''' spin system. A reasonable extrapolation is to assume that the ^1H spectrum of the actual AA'XX'X''X'''X''''X'''''X''''''X''''''' spin system consists of a nine-line pattern with the same splitting for $J_{P-O-P} > 42$ Hz.

The following set of coupling constants was used, although simulations on the smaller spin systems did not require all the values: $^2J_{P-H}$, 11; $^3J_{P-H}$, 3.7 (also could be $^4J_{P-H}$); $^1J_{Pt-H}$, 884; $^2J_{Pt-H}$, 103; $^3J_{H-H}$, 26; $^2J_{P-O-P}$, 45 (any value >42 Hz gives the same result); $^1J_{Pt-P}$, 2190; $^1J_{Pt-Pt}$, 8000 Hz. All other coupling constants were defined as 0.01 Hz. Very similar systems containing ≤ 10 spins have been completely simulated;[5] these simulations indicate that P-P couplings occur through the P-Pt-P and P-Pt-Pt-P linkages as well as through the P-O-P linkage. The magnitudes of the P-P couplings other than via the P-O-P bridge could not be determined in the present work, however. All simulations are available as supplementary material.

(1) Permanent address: The J. Heyrovský Institute of Physical Chemistry and Electrochemistry, Vlašská 9, 11840 Prague, Czechoslovakia.
(2) Roundhill, D. M. *J. Am. Chem. Soc.* **1985**, *107*, 4354-4356.
(3) Marshall, J. L.; Stiegman, A. E.; Gray, H. B. *Excited States and Reactive Intermediates*; Lever, A. B. P., Ed.; ACS Symposium Series 307; American Chemical Society: Washington, DC, 1986; pp 166-176.
(4) Vlček, Jr., A.; Gray, H. B. *J. Am. Chem. Soc.* **1987**, *109*, 286-287; *Inorg. Chem.* **1987**, *26*, 1997-2001.
(5) King, C.; Roundhill, D. M.; Dickson, M. K.; Fronczek, F. R. *J. Chem. Soc., Dalton Trans.*, in press.

0002-7863/87/1509-5233$01.50/0